Published in final edited form as:
Behav Brain Res. 2012 February 1; 227(1): 233–240. doi:10.1016/j.bbr.2011.10.026.

Neural Intrinsic Connectivity Networks Associated with Risk Aversion in Old Age

S. Duke Han[a], **Patricia A. Boyle**[a,c], **Konstantinos Arfanakis**[b,c,e], **Debra A. Fleischman**[a,c], **Lei Yu**[c,d], **Emily C. Edmonds**[a], and **David A. Bennett**[c,d]

[a]Department of Behavioral Sciences, Rush University Medical Center, Chicago, IL 60612, USA

[b]Department of Biomedical Engineering, Illinois Institute of Technology, Chicago, IL 60616, USA

[c]Rush Alzheimer's Disease Center, Rush University Medical Center, Chicago, IL 60612, USA

[d]Department of Neurological Sciences, Rush University Medical Center, Chicago, IL 60612, USA

[e]Department of Radiology, Rush University Medical Center, Chicago, IL 60612, USA

Abstract

Risk aversion is associated with several important real world outcomes. Although the neurobiological correlates of risk aversion have been studied in young persons, little is known of the neurobiological correlates of risk aversion among older persons. Resting-state functional MRI data were collected on 134 non-demented participants of the Rush Memory and Aging Project, a community-based cohort study of aging. Risk aversion was measured using a series of standard questions in which participants were asked to choose between a certain monetary payment ($15) versus a gamble in which they could gain more than $15 or gain nothing, with potential gains varied across questions. Participants determined to be "high" (n=27) and "low" (n=27) in risk aversion were grouped accordingly. Using a spherical seed region of interest in the anterior cingulate cortex, voxel-wise functional connectivity network similarities were observed in bilateral frontal, anterior and posterior cingulate, insula, basal ganglia, temporal, parietal, and thalamic regions. Differences in functional connectivity were observed such that those low in risk aversion had greater connectivity to clusters in the superior, middle, and medial frontal regions, as well as cerebellar, parietal, occipital, and inferior temporal regions. Those high in risk aversion had greater connectivity to clusters in the inferior and orbital frontal, parahippocampal, and insula regions, as well as thalamic, parietal, precentral gyrus, postcentral gyrus, and middle temporal regions. Similarities and differences in functional connectivity patterns may reflect the historical recruitment of specific brain regions as a network in the active processing of risk in older adults.

Keywords

risk aversion; aging; resting state fMRI; functional connectivity; anterior cingulate

Corresponding Author: S. Duke Han, PhD, Department of Behavioral Sciences, 1645 W. Jackson Blvd. Ste. 400, Chicago, IL 60612; 312-942-2893 (phone), 312-942-4990 (fax), Duke_Han@rush.edu.

DISCLOSURES

There were no actual or potential conflicts of interest for any of the authors.

1. INTRODUCTION

Risk aversion is associated with a wide range of meaningful behaviors. Attitudes toward risk may influence financial and healthcare decisions and even health practices [1,2]. For example, persons who are risk averse tend to exhibit fewer negative health behaviors (e.g., are less likely to smoke cigarettes) [3] but often make poorer financial decisions (e.g., choose “safe” but low yield investments) compared to those less risk averse. Recent work suggests that decision-making in risky situations may be an important function in old age [29], yet the neurobiologic substrate of risk aversion in old age remains unknown. Given that risk aversion is an important determinant of a variety of behaviors, many of which are essential to successful aging, knowledge of the neurobiologic substrate of risk aversion in old age may have significant public health implications.

One approach which shows promise in illuminating the functional neurobiologic substrate of a behavioral characteristic is resting-state functional magnetic resonance imaging (r-sfMRI). This approach assesses functional connectivity of particular brain networks by detecting gray matter regions that exhibit high temporal coherence of low frequency fluctuations [5]. High temporal coherence of brain regions is presumed to represent a functionally associated network, and networks may differ based on predetermined characteristics. Resting-state fMRI has been recently used with older populations to delineate salient networks associated with aging and cognitive decline [e.g., 6,7]. However, to our knowledge, this approach has yet to be used to study risk aversion in old age.

In this study, we examined the neurobiologic substrate of risk aversion among non-demented older persons using resting-state functional MRI. Participants were from the Rush Memory and Aging Project, a large clinicopathologic, longitudinal, and community-based study of aging. All participants underwent detailed clinical evaluations and assessments of risk aversion using standard behavioral economics questions in which they were asked to choose between a guaranteed payment of $15 or a gamble in which they could either gain various sums greater than $15 or nothing at all. Utilizing resting-state functional magnetic resonance imaging [8,9] we sought to examine potential differences in neural intrinsic connectivity networks among participants in the highest 20 percent (n=27) and lowest 20 percent (n=27) in risk aversion. Previous task-related fMRI studies have identified brain regions that appear to be active during situations of risk, with some regions more active for risk-averse persons and others more active for non-risk averse or risk-seeking persons [17, 19, 26–29]. If the regions involved vary by risk aversion preference, then over time persons high or low in risk aversion may invoke different brain networks of regions when making risky choices, and these networks may gradually become more functionally connected in the baseline state as implied by recent work [36]. Because of this, we examined the similarities and differences in the functional connectivity of brain regions among those low and high in risk aversion in accordance with the assumption that these similarities and differences may reflect the historical recruitment of specific brain regions as a network in the active processing of risk in older adults.

2. METHODS

2.1. Participants and Procedures

The current study included participants from the Rush Memory and Aging Project, a community-based clinicopathologic cohort study of aging and dementia [10]. Participants come from approximately 40 residential facilities across the greater Chicago metropolitan area, including subsidized senior housing facilities, retirement communities, retirement homes, local churches, and other community organizations. All procedures were approved by the Rush Institutional Review Board.

The Rush Memory and Aging Project has a rolling admission that started in 1997. Brain imaging was initiated in 2008. At the time of analyses, 1299 participants had enrolled and completed their baseline evaluation, 443 died, and 77 refused further participation. Of the remaining 779, 260 had MRI contraindications or were unable to sign informed consent, leaving 519 eligible for scanning. Of these, 155 (29.9%) refused scanning, 214 were scanned, and the remaining 150 were still being scheduled for scanning. Of the 214 that were scanned, 1 was excluded due to dementia, and 134 completed an assessment of risk aversion, as part of a separate substudy on neuroconomics of aging, and were eligible for these analyses. For the purpose of comparing those high and low in risk aversion, we comprised two subgroups drawn from the 134 participants (i.e., n=27, the highest 20% and n=27, the lowest 20% of the sample).

Diagnostic classification was performed according to standard procedures [10,11]. The clinical diagnosis of dementia and Alzheimer's disease follows the recommendations of the joint working group of the NINCDS/ADRDA [12] as previously described [11]. These criteria require a loss of function in memory and at least one other cognitive ability.

2.2. Assessment of risk aversion

Risk aversion was assessed with 10 questions used in standard behavioral economics approaches. An example of one of these questions is "Would you prefer $15 for sure, OR a coin toss in which you will get $[an amount greater than $15] if you flip heads or nothing if you flip tails?" Possible gains ranged from $21.79 to $151.19 and gain amounts were varied across questions. Questions were developed in such a manner that any gamble that offered a potential gain of $30 resulted in the same long run average or expected utility, and any gamble that was over $30 resulted in a greater than expected utility. Therefore, any gamble over $30 was a "preferred" choice.

2.3. Image Acquisition and Processing

MRI scans were conducted on a 1.5 Tesla clinical scanner (General Electric, Waukesha, WI), equipped with a standard quadrature head coil, located within the community of the sample. High data quality was ensured through daily quality assurance tests. High-resolution T1-weighted anatomical images were collected with a 3D magnetization-prepared rapid acquisition gradient-echo (MPRAGE) sequence with the following parameters: TR = 6.3 ms; TE = 2.8 ms; preparation time = 1000 ms; flip angle = 8°; 160 sagittal slices; 1 mm slice thickness; field of view (FOV) = 24 cm × 24 cm; acquisition matrix 224 × 192, reconstructed to a 256 × 256 image matrix; scan time = 10 min and 56 secs. Two copies of the T1-weighted data were acquired on each subject. Resting state MRI data was acquired using a 2D spiral in/out echo-planar imaging (EPI) sequence with the following parameters: TR = 2000 ms; TE = 33 ms; flip angle = 85°; 26 oblique axial slices; 5 mm slice thickness; acquisition/reconstruction matrix 64 × 64; FOV = 24 cm × 24 cm; 240 time-points/volumes; scan time = 8 min.

The skull was removed from each structural MRI dataset using FreeSurfer's Hybrid Watershed Algorithm [13]. Structural scans were also manually edited when necessary to remove residual non-brain material. Brain segmentation into gray matter, white matter and CSF was also performed using FreeSurfer (http://surfer.nmr.mgh.harvard.edu/). Whole brain volume was also derived, and thus proportions of each compartment were calculated.

The first 5 image volumes of resting state data were discarded at the scanner to avoid using data collected before reaching signal equilibrium. Images were reconstructed on Linux machines from the acquired k-space data [14]. Using the Statistical Parametric Mapping software [15; http://www.fil.ion.ucl.ac.uk/spm/] version 8 (SPM8), all volumes were

corrected for motion, co-registered to the high-resolution T1-weighted data, and spatially normalized to the Montreal Neurological Institute (MNI) template. The normalized image volumes were spatially smoothed with a 4mm full-width halfmaximum (FWHM) Gaussian kernel. Next, a band-pass filter of 0.01 to 0.08 Hz was applied to the data in temporal frequency space to minimize low-frequency signal drift and high frequency variations due to cardiac and respiratory effects. In order to remove any residual effects of motion and other non-neuronal factors, 6 head motion parameters, as well as parameters for the white matter signal, global mean signal, and cerebrospinal fluid signal were used as nuisance variables [16] in functional connectivity analysis using the Resting-State fMRI Data Analysis Toolkit (REST: http://restfmri.net/forum/REST). As an additional quality-control post-processing measure, independent component analysis (ICA) was conducted using the MELODIC software package from FSL (http://www.fmrib.ox.ac.uk/fsl/) to confirm regression of unwanted nuisance variables and identify other potential nuisance variables unaccounted in the REST regression. More specifically, ICA was utilized to determine if participant scans showed additional evidence of nuisance variables such as residual head motion. If a participant's scan was visually inspected and found to have significant residual contributions from nuisance factors after our regression procedures, the participant was dropped from further analyses.

We viewed the anterior cingulate and the network of regions associated with it as an essential network for cognitive and affective processes involved in decision-making based on previous literature in young persons [e.g., 17, see 26 for a review]. The anterior cingulate is anatomically and functionally associated with multiple regions implicated in decision-making, including the ventromedial prefrontal cortex, the medial orbitofrontal cortex, the lateral prefrontal cortex, amygdala, premotor regions, and the thalamus [27]. Lesion studies in monkeys have suggested that the anterior cingulate cortex is an essential region for determining response to rewards [28]. Therefore we chose to focus on this network as our primary network of investigation. A spherical seed ROI with a radius of 8mm was prescribed in the anterior cingulate cortex, with MNI coordinates of x=0, y=39, z=−4 in order to interrogate functional connectivity in a network of brain regions associated with risk aversion. The size and location of the seed ROI was determined in consideration of previous work [9]. A mean signal time course for the seed was calculated and used as a reference. Cross-correlation analysis was then conducted between the reference signal time course and the time series of each other voxel in the brain. The voxels showing significant functional connectivity to the anterior cingulate seed ROI were identified as those voxels whose cross-correlation differed significantly (alpha=0.005) from 0, based on one-sample t-tests applied to Fisher's z-transformation of the correlation. Seed-based functional connectivity analysis was conducted with the Data Processing Assistant for Resting-State fMRI (DPARSF; http://restfmri.net/forum/DPARSF) and SPM8.

2.4. Statistical Analyses

Statistical analyses proceeded in several steps. First, the risk aversion parameter γ (gamma) was estimated from participants' responses on all 10 risk aversion questions, which included both safe payoffs and gamble options. The gamble option payoff for *i* th participant at *j* th question, GP_{ij}, was defined as,

$$GP_{ij}=\frac{0.5 \times Gain_j^{1-\gamma_i}}{1-\gamma_i}$$

where $Gain_j$ was the gamble gain for *j* th question, and γ_i the risk aversion parameter for *i* th participant.

Similarly, the safe option payoff for *i* th participant at *j* th question, SP_{ij}, was defined as,

$$SP_{ij}=\frac{Safe_j^{1-\gamma_i}}{1-\gamma_i}$$

where $Safe_j$ was the safe gain for *j* th question, and γ_i the risk aversion parameter for *i* th participant.

The probability of subject *i* choosing the gamble at question *j*, p_{ij}, assumes to be dependent on the difference between GP_{ij} and SP_{ij}, which is linked through a logistic function,

$$\text{logit}\left(P(Y_{ij}=1)\right)=GP_{ij}-SP_{ij}$$

Substituting GP_{ij} and SP_{ij}, we have,

$$\text{logit}\left(P(Y_{ij}=1)\right)=\frac{0.5\times Gain^{1-\gamma_i}-Safe^{1-\gamma_i}}{1-\gamma_i}$$

Here Y_{ij} is the item response from the *i* th participant to the *j* th question. The risk aversion estimate for each individual participant was obtained by maximizing the likelihood function constructed based upon this logistic model. These methods are further described in a previous report [30].

From this statistical estimation of risk aversion, the 27 individuals highest in gamma (high in risk aversion) and the 27 individuals lowest in gamma (low in risk aversion) comprised two groups drawn from 134 participants who completed both the risk aversion assessment and neuroimaging (i.e., the highest 20% and lowest 20% of the sample). We then examined between-group differences in demographic variables (age, education, sex, MMSE, race), brain volumetry (total gray matter volume), and risk aversion gamma (low gamma versus high gamma) using two-tailed t-tests (age, education, MMSE, total gray matter volume) or Chi-square tests (sex, race). We then verified the functional connectivity of the anterior cingulate cortex to other regions by determining within-group whole brain z-transformed functional clusters of significance for both risk aversion categories (low gamma and high gamma) after covarying for the effects of age and total gray matter volume. These characteristics were used as covariates since both groups differed with respect to age and total gray matter volume is known to commonly effect fMRI signal in the brain. In order to control for multiple comparisons, within-group whole brain functional imaging results were controlled by employing a false discovery rate (FDR) of $p<0.05$, cluster size > 5 voxels, p-value < 0.004. Finally, we conducted voxel-wise, between-group t-test comparisons of z-transformed functional connectivity values (low gamma versus high gamma) while adjusting for the effects of age and total gray matter volume. The chance of spurious findings was controlled by utilizing the same parameters as our within group analyses (cluster size > 5 voxels, p-value < 0.004).

3. RESULTS

3.1. Demographic and Brain Volumetry Differences Between Those Low and High in Risk Aversion

Demographic and brain volumetry characteristics are shown in Table 1. Most participants were white. Our high and low risk aversion groups significantly differed by age. Because of this, age was used as a covariate in addition to overall structural gray matter for all analyses. No other group differences were observed for education level, gender, or overall structural gray matter.

3.2. Within-Group Resting-State Functional Connectivity of the Anterior Cingulate Cortex in Those Low and High in Risk Aversion

Seeding the anterior cingulate cortex yielded a network of functionally related regions consistently observed by other functional neuroimaging studies after controlling for age and total gray matter volume among those high and low in risk aversion (Figure 1). Within-group analyses revealed large clusters of significance centering in bilateral frontal, temporal, and parietal regions, many of which are consistent with the Default Mode Network, for both risk aversion groups (Table 2). However, those low in risk aversion exhibited a large cluster of significance (t=20.1137) including bilateral frontal gyrus, anterior cingulate, basal ganglia, insula, medial temporal gyrus, and thalamus regions; a large cluster of significance (t=6.7369) including bilateral temporal, parietal, posterior cingulate, and thalamus regions; and smaller clusters of significance in the right middle and superior temporal gyri (t=5.3182), right middle temporal gyrus (t=4.5114), left medial and superior temporal gyrus (t=4.4459), right transverse temporal gyrus (t=3.7896), left insula (t=3.5210), left middle temporal gyrus (t=3.4030), right cerebellum (t=3.4028), left middle and superior temporal gyri (t=3.2940), right posterior cingulate (t=3.2873 and t=3.2484), right superior temporal gyrus (t=3.2454 and t=3.1343), left parahippocampal gyrus (t=3.2340), and left middle temporal gyrus (t=3.1224). Those high in risk aversion exhibited a large cluster of significance (t=18.8969) including bilateral frontal, temporal, parietal, basal ganglia, insula, anterior cingulate, and posterior cingulate regions; and smaller clusters of significance in the left superior, middle, and inferior temporal gyri (t=4.5704), right putamen (t=4.1986), right parietal region (t=3.8723), right inferior frontal gyri (t=3.6893), right cuneus (t=3.5766 and t=3.3529), left superior tempora gyrus (t=3.5061), left thalamus (t=3.3787), and right thalamus (t=2.9456).

3.3. Between-Group Resting-State Functional Connectivity Network Similarities in Those Low and High in Risk Aversion

Between-group analyses of functional connectivity network similarities revealed multiple overlapping regions of functional connectivity between participants low and high in risk aversion (Figure 2; Table 3). Two large overlapping clusters were observed, one in the anteriomedial region and the other in the posteriomedial region. The anteriomedial cluster included bilateral frontal, anterior cingulate, basal ganglia, insula, medial temporal, and thalamic regions (t=20.1137). The posteriomedial cluster included bilateral temporal, parietal, posterior cingulate, and thalamic regions (t=6.7369). Other regions of overlap included right (t=5.3182) and left (two clusters: t=4.4459 and t=3.2940) middle and superior temporal regions, right (t=4.5114) and left (three clusters: t=4.0790, t=3.4030, and t=3.1224) middle temporal regions, right transverse temporal (t=3.7896), left insula (t=3.5210), right cerebellum (t=3.4028), right posterior cingulate (two clusters: t=3.2873 and t=3.2484), right superior temporal (t=3.2454), left parahippocampal (t=3.2340), and right superior temporal (t=3.1343).

3.4. Between-Group Resting-State Functional Connectivity Network Differences in Those Low and High in Risk Aversion

Between-group contrasts revealed multiple regions of functional connectivity differences between participants low and high in risk aversion (Figure 3). Persons who were low in risk aversion had greater connectivity between the anterior cingulate and clusters in the left dorsolateral prefrontal region (two clusters: t=4.0531 and t=3.1752), right dorsolateral prefrontal region (two clusters: t=4.0050 and t=3.9568), left superior frontal gyrus (t=3.8265 and t=3.6092), right superior medial frontal gyrus (t=3.5877), right cerebellum (t=3.7805), left superior parietal gyrus (t=3.7618), right middle occipital gyrus (t=3.6168), right inferior occipital gyrus (t=3.1640) and right inferior temporal gyrus (t=3.1034) when compared to those high in risk aversion. By contrast, persons who were high in risk aversion had greater functional connectivity between the anterior cingulate and right parahippocampal gyrus (t=4.0246), right inferior frontal gyrus (t=3.5972), left postcentral gyrus (t=3.5954), left parahippocampal gyrus (t=3.5574), left inferior parietal gyrus (t=3.3627), right orbital frontal gyrus (t=3.3559), right middle frontal gyrus (t=3.3409), left insula (t=3.3409), left precentral gyrus (t=3.3084), right thalamus (t=3.2627), right middle temporal gyrus (t=3.0381) and left inferior parietal gyrus (t=2.8866) when compared to those low in risk aversion (Table 4).

4. DISCUSSION

We examined the neurobiological correlates of risk aversion in more than 50 older persons using resting state fMRI and hypothesized that we would observe network similarities and differences between risk aversion groups. Two large clusters of regional overlap were observed, one in the anteriomedial cortices and one in the posteriomedial cortices. The anteriomedial cluster includes many regions that have been implicated in prior neuroimaging studies of decision-making [17–23, 26–29]. Differences in network functional connectivity were also observed. Middle frontal, and specifically dorsolateral prefrontal, regions have been shown to be active in risk evaluation situations [26] as well as reasoning and problem-solving [32]. We observed these regions being more functionally associated with those low in risk-aversion. Inferior and orbital frontal [17] and insular [19] region activity has been associated with risk aversion in task-related fMRI investigations. More specifically, inferior and orbital frontal regions appear to process abstract rewards and punishments [33], while insula activity interestingly appears to be associated with the perception of pain and noxious stimuli [34]. We observed greater connectivity of these structures among those high in risk aversion. Mesial prefrontal regions appear to be associated with anticipated gain probability [20], while the anterior cingulate [17] and mesolimbic structures such as the nucleus accumbens appear to be associated with gain magnitude [20], risky choices, and suboptimal financial choices due to risk-seeking behavior [18]. We observed in older adults low in risk aversion relatively greater connectivity between anterior cingulate and superior and mesial frontal regions. Activity in parahippocampal regions has been shown to directly correlate with risk taking behavior [21] with increased activity correlating with risk taking behavior and decreased activity correlating with risk averse behavior. Our results suggest that these regions may functionally play a more important role in risk averse behavior versus risk seeking behavior. Inferior parietal activity has been implicated in other studies of risk averse behavior [22], and we observed functional connectivity of the anterior cingulate and the inferior parietal region in older adults high in risk aversion. The inferior temporal cortex has been shown to project sensory and object information into the prefrontal cortex [23], and this may reflect why this region may serve a greater functionally associated role in individuals low in risk aversion. Overall, observed similarities and differences in functional connectivity patterns may reflect the historical recruitment of specific brain regions as a network in the active processing of risk in older adults.

The anteriormedial cluster, posteriomedial cluster, and some of the other regions of similarity (temporal, parahippocampal, cerebellum) have also been implicated as part of the Default Mode Network [9, 31]. The Default Mode Network is a network of brain regions that remains active during times when an individual is not actively engaged in an overt cognitive task, and changes in this network have been implicated in the progression of Alzheimer's dementia [6]. Because seed regions in the anterior cingulate have been previously used to interrogate the Default Mode Network, our results are therefore consistent with previous reports. However, a qualitative review of our results in comparison to previous reports of the Default Mode Network suggests even greater prominence of the anterior portion of this network. A hypothesized function of the Default Mode Network is that it is involved in "internal mentation", and that the anterior portion of the network (e.g., anterior cingulate, ventromedial prefrontal cortex) is more involved in self-referential future projection while the posterior portion of the network (e.g., posterior cingulate, parahippocampal regions) is involved in integrating autobiographical memory into current processing [31]. Certainly the prominence of the anterior portion of this network in our results may highlight its importance in the context of risk aversion in older adults.

Several of the observed regions of difference (e.g., left and right parahippocampal, left inferior parietal, right inferior temporal, medial frontal) are also associated with the Default Mode Network. These differences may reflect differential recruitment of portions of the Default Mode Network by risk aversion status. Changes in the functional connectivity of the Default Mode Network have been observed with self-referential processing [24] and some personality styles [25]. It is therefore reasonable to assume that risk aversion preference may be associated with changes in the functional connectivity of portions of the Default Mode Network over time.

Our results suggest that there is a shared network of regions functionally associated among older adults that appears to be important in risk aversion behavior. Those high and low in risk aversion generally show significant overlap in these regions, which include the anterior cingulate, ventromedial prefrontal cortex, basal ganglia structures, insula, medial temporal, thalamic, posterior cingulate, and parietal regions. Notably, many of these structures have been implicated as important in task-related fMRI studies of risk aversion and decision-making [17, 26–29] as well as the Default Mode Network [6, 9, 24–25, 31]. Although there was significant overlap between risk-averse groups, differences were also observed by high and low risk aversion. These differences argue for a greater association of particular structures to this shared network of decision-making by risk aversion preference. Older adults low in risk aversion appear to have more integration of regions involved in planning and problem-solving (e.g., dorsolateral prefrontal cortex), and older adults high in risk aversion appear to have more integration of regions involved in the experience of rewards and punishments (e.g., orbital frontal) and noxious stimuli (e.g., insula). These regional differences are the largest differences based on cluster size. One hypothetical distinction between groups based on the present results is that older adults low in risk aversion are more apt to look at a decision in a more logical and reasoned manner, while older adults high in risk aversion are more sensitive to the noxious aspects of a risk and therefore chose the "safe" option. However, this hypothesis needs to be systematically tested.

To our knowledge, only two previous task-related studies have examined the neurobiological basis of risk aversion in older persons [29, 35]. In one study [29], older adults made more suboptimal choices than younger adults when choosing risky assets, and the age-related effect was mediated by activity in the nucleus accumbens. We observed basal ganglia structures as a shared region of functional connectivity between group low and high in risk aversion, consistent with the notion of it being an important brain network component for risk aversion processing in older adults. In another study [35], older adults

were observed to make more risk averse choices compared to young adults, and this corresponded with greater activation in right insula and right orbitalfrontal cortex in older adults. We observed greater connectivity of orbitofrontal and insula regions in older participants high in risk aversion. Our study extends this knowledge by implicating the functional connectivity of a subset of other brain regions that may differentiate older adults by risk aversion preference.

Our study presents two contributions to the literature. First, we utilized resting-state fMRI approaches to explore the functional architecture of risk aversion. While previous studies have utilized task or event-related fMRI to delineate the activity of particular brain structures while performing a specific risk aversion task, resting-state fMRI allows for the identification of a network of regions functionally associated at baseline (i.e., “at rest”). Our intrinsic connectivity network fMRI findings in conjunction with previous task-related fMRI work support the notion of a shared network of regions functionally primed to process risk among older adults, and a subset of functionally connected regions that may differentiate risk aversion preference and behavior among older adults. Second, we are not aware of a prior study that has investigated the functional connectivity correlates of risk aversion in older persons. The consistency of our findings with previous literature suggests that the neural systems associated with risk aversion may be similar in younger and older persons; however, more investigation is needed to determine whether this is indeed the case.

Limitations of the present study include our restriction to the anterior cingulate cortex as a seed region of interest for our functional connectivity approach. Certainly it would be interesting to examine other seed ROIs to interrogate other intrinsic connectivity networks in relation to risk aversion in old age; however, we viewed the anterior cingulate and the network of regions anatomically and functionally associated with it as an essential network for financial decision-making based on previous literature [e.g., 17, see 26 for a review]. Therefore we chose to focus on this network as our primary network of investigation. Another limitation is that participants did not use real money. Because this is an optional component to a longitudinal cohort study for which no monies are provided for any component, the introduction of money could be problematic for other study components. Also, we did not directly assess gain and loss sensitivity. Measurement of this would have provided us the opportunity to make inferences of the functional connectivity differences between groups. A notable limitation is our inability to investigate age effects. There were no younger samples to use as a comparison group for our older sample. Hence, we were not able to discern whether our observations were due to age effects or other factors. Other limitations include the relatively small sample size; an interval of months, on average, from the time of the risk aversion assessment and neuroimaging; and the fact that we used an estimation of risk aversion.

Strengths of the present study include use of a community-based sample in whom risk aversion had been measured via a standard behavioral economics approach, the advanced age of the cohorts, and the ability to control for factors such as age and total gray matter volume. Results suggest there is considerable overlap in the functional connectivity of regions to the anterior cingulate among older adults who differ by risk aversion preference; however, there are also significant regional and network differences. Further studies are needed to further examine the network dynamics of these and clarify other correlates of risk aversion in older persons.

HIGHLIGHTS

- We examined neural correlates of risk aversion in old age using resting-state fMRI.

- Risk aversion status was determined using neuroeconomic approaches.
- Similarities and differences in functional connectivity were associated with high/low risk aversion.
- Those high in risk aversion show greater functional connectivity of a network of regions including the orbitofrontal cortex, insula, and parahippocampal gyri.
- Those low in risk aversion show greater functional connectivity of a network of regions including the dorsolateral prefrontal, superior parietal, and inferior temporal cortex.

Acknowledgments

Supported by National Institute on Aging grants R01AG17917 and R01AG33678, the Illinois Department of Public Health, and The Marsha K. Dowd Philanthropic Fund. We gratefully acknowledge the assistance of Dr. Randy Buckner, Dr. Gary Glover, and Dr. Jeffrey Rosengarten with this project. We thank Niranjini Rajendran, M.S., and Woojeong Bang, M.S., for image post-processing and statistical analyses. We also thank the Rush Memory and Aging Project staff and participants.

REFERENCES

1. Barksy RB, Kimball MS, Juster FT, Shapiro MD. Preference parameters and behavioral heterogeneity: An experimental approach in the Health and Retirement Survey. Q J Econ. 1997; 112:537–579.
2. Kimball M, Sahm C, Shapiro M. Imputing risk tolerance from survey responses. J Am Stat Assoc. 2009; 103:1028–1038. [PubMed: 20407599]
3. Anderson LR, Melor JM. Are risk preferences stable? Comparing an experimental measure with a validated survey-based measure. College of William and Mary Department of Economics. 2008 Working Paper Number 74.
4. Deakin J, Aitken M, Robbins T, Sahakian BJ. Risk taking during decision-making in normal volunteers changes with age. J Int Neuropsychol Soc. 2004; 10:590–598. [PubMed: 15327737]
5. Van Dijk KRA, Hedden T, Venkatataman A, Evans KC, Lazar SW, Buckner RL. Intrinsic functional connectivity as a tool for human connectomics: Theory, properties, and optimization. J Neurophysiol. 2010; 103:297–321. [PubMed: 19889849]
6. Buckner RL, Synder AZ, Shannon BJ, LaRossa G, Sachs R, Fotenos AF, Sheline YI, Klunk WE, Mathis CA, Morris JC, Mintun MA. Molecular, structural, and functional characterization of Alzheimer's disease: Evidence for a relationship between default activity, amyloid, and memory. J Neurosci. 2005; 25:7709–7717. [PubMed: 16120771]
7. Greicius MD, Srivastava G, Reiss AL, Menon V. Default-mode network activity distinguishes Alzheimer's disease from healthy aging: Evidence from functional MRI. Proc Natl Acad Sci. 2004; 101:4637–4642. [PubMed: 15070770]
8. Raiche ME, MacLeod AM, Snyder AZ, Powers WJ, Gusnard DA, Shulman GL. A default mode of brain function. Proc Natl Acad Sci. 2001; 98:676–682. [PubMed: 11209064]
9. Greicius MD, Krasnow B, Reiss AL, Menon V. Functional connectivity in the resting brain: A network analysis of the default mode hypothesis. Proc Natl Acad Sci. 2003; 100:253–258. [PubMed: 12506194]
10. Bennett DA, Schneider JA, Buchman AS, Mendes de Leon C, Bienias JL, Wilson RS. The Rush Memory and Aging Project: Study design and baseline characteristics of the study cohort. Neuroepidemiology. 2005; 25:163–175. [PubMed: 16103727]
11. Bennett DA, Schneider JA, Aggarwal NT, Arvanitakis Z, Shah RC, Kelly JF, Fox JH, Cochran EJ, Arends D, Treinkman AD, Wilson RS. Decision rules guiding the clinical diagnosis of Alzheimer's disease in two community-based cohort compared to standard practice in a clinic-based cohort study. Neuroepidemiology. 2006; 27:169–176. [PubMed: 17035694]

12. McKhann G, Drachman D, Folstein M, Katzman R, Price D, Stadlan EM. Clinical diagnosis of Alzheimer's disease. Neurology. 1984; 34:939. [PubMed: 6610841]
13. Segonne F, Dale AM, Busa E, Glessner M, Salat D, Hahn HK, Fischl B. A hybrid approach to the skull stripping problem in MRI. Neuroimage. 2004; 22:1060–1075. [PubMed: 15219578]
14. Glover GH, Thomason ME. Improved combination of spiral-in/out images for BOLD fMRI. Magn Reson Med. 2004; 51:863–868. [PubMed: 15065263]
15. Friston KJ, Passingham RE, Hutt JG, Heather JD, Sawle GV, Frackowiak RSJ. Spatial registration and normalization of images. Hum Brain Mapp. 1995; 3:165–189.
16. Buckner RL, Sepulcre J, Talukdar T, Krienen FM, Liu H, Hedden T, Andrews-Hanna JR, Sperling RA, Johnson KA. Cortical hubs revealed by intrinsic functional connectivity: Mapping, assessment of stability, and relation to Alzheimer's disease. J Neurosci. 2009; 29:1860–1873. [PubMed: 19211893]
17. Christopoulos GI, Tobler PN, Bossaerts P, Dolan RJ, Schultz W. Neural correlates of value, risk, and risk aversion contributing to decision making under risk. J Neurosci. 2009; 29:12574–12583. [PubMed: 19812332]
18. Kuhnen CM, Knutson B. The neural basis of financial risk taking. Neuron. 2005; 47:763–770. [PubMed: 16129404]
19. Paulus MP, Rogalsky C, Simmons A, Feinstein JS, Stein MB. Increased activation in the right insula during risk-taking decision making is related to harm avoidance and neuroticism. Neuroimage. 2003; 19:1439–1448. [PubMed: 12948701]
20. Knutson B, Taylor J, Kaufman M, Peterson R, Glover G. Distributed neural representation of expected value. J Neurosci. 2005; 25:4806–4812. [PubMed: 15888656]
21. Engelmann JB, Tamir D. Individual differences in risk preference predict neural responses during financial decision-making. Brain Res. 2009; 1290:28–51. [PubMed: 19576868]
22. Tom SM, Fox CR, Trepel C, Poldrack RA. The neural basis of loss aversion in decision-making under risk. Science. 2007; 315:515–518. [PubMed: 17255512]
23. Kreiman G, Hung CP, Kraskov A, Quiroga RQ, Poggio T, DiCarlo JJ. Object selectivity of local field potentials and spikes in the macaque inferior temporal cortex. Neuron. 2006; 49:433–445. [PubMed: 16446146]
24. Van Buuren M, Gladwin TE, Zandbelt BB, Kahn RS, Vink M. Reduced functional coupling in the default-mode network during self-referential processing. Hum Brain Mapp. 2010; 31:1117–1127. [PubMed: 20108218]
25. Sheng T, Gheytanchi A, Aziz-Zadeh L. Default Network Deactivations Are Correlated with Psychopathic Personality Traits. PLoS ONE. 2010; 5(9):e12611. [PubMed: 20830290]
26. Rushworth MFS, Noonan MP, Boorman ED, Walton ME, Behrens TE. Frontal cortex and Reward-Guided Learning and Decision-Making. Neuron. 2011; 70:1054–1069. [PubMed: 21689594]
27. Van Hoesen, GW.; Morecraft, RJ.; Vogt, BA. Connections of the monkey cingulate cortex. In: VOGT, BA.; Gabriel, M., editors. Neurobiology of Cingulate Cortex and Limbic Thalamus. Boston: Birkhauser;
28. Kennerley SW, Walton ME, Behrens TE, Buckley MJ, Rushworth MF. Optimal decision making and the anterior cingulate. Nat Neurosci. 2006; 9:940–947. [PubMed: 16783368]
29. Samanez-Larkin GR, Kuhnen CM, Yoo DJ, Knutson B. Variability in nucleus accumbens activity mediates age-related suboptimal financial risk taking. The Journal of Neurosciences. 2010; 30(4): 1426–1434.
30. Boyle PA, Yu L, Buchman AS, Laibson DI, Bennett DA. Cognitive function is associated with risk aversion in community-based older persons. BMC Geriatrics. (in press).
31. Buckner RL, Andrews-Hanna JR, Schacter DL. The brain's default network: Anatomy, function, and relevance to disease. Annals NY Acad Sci. 2008; 1124:1–38.
32. Kroger JK, Sabb FW, Fales CL, Bookheimer SY, Cohen MS, Holyoak KJ. Recruitment of anterior dorsolateral prefrontal cortex in human reasoning: a parametric study of relational complexity. Cereb Cortex. 2002; 12(5):477–485. [PubMed: 11950765]
33. O'Doherty J, Kringelbach ML, Rolls ET, Hornak J, Andrews C. Abstract reward and punishment representations in the human orbitofrontal cortex. Nature Neuroscience. 2001; 4(1):95–102.

34. Ostrowsky K, Magnin M, Ryvlin P, Isnard J, Guenot M, Mauguiere F. Representation of pain and somatic sensation in the human insula: A study of responses to direct electrical cortical stimulation. Cereb Cortex. 2002; 12(4):376–385. [PubMed: 11884353]

35. Lee TMC, Leung AWS, Fox PT, Gao J-H, Chan CCH. Age-related differenes in neural activities during risk taking as revealed by functional MRI. SCAN. 2008; 3:7–15. [PubMed: 19015090]

36. de Bie HMA, Boersma M, Adriaanse S, Veltman DJ, Wink AM, Roosendaal SD, Barkhof F, Stam CJ, Oostrom KJ, Delemarre-van de Waal HA, Sanz-Arigita EJ. Resting-state networks in awake five- to eight-year old children. Human Brain Mapping. 2011 in press.

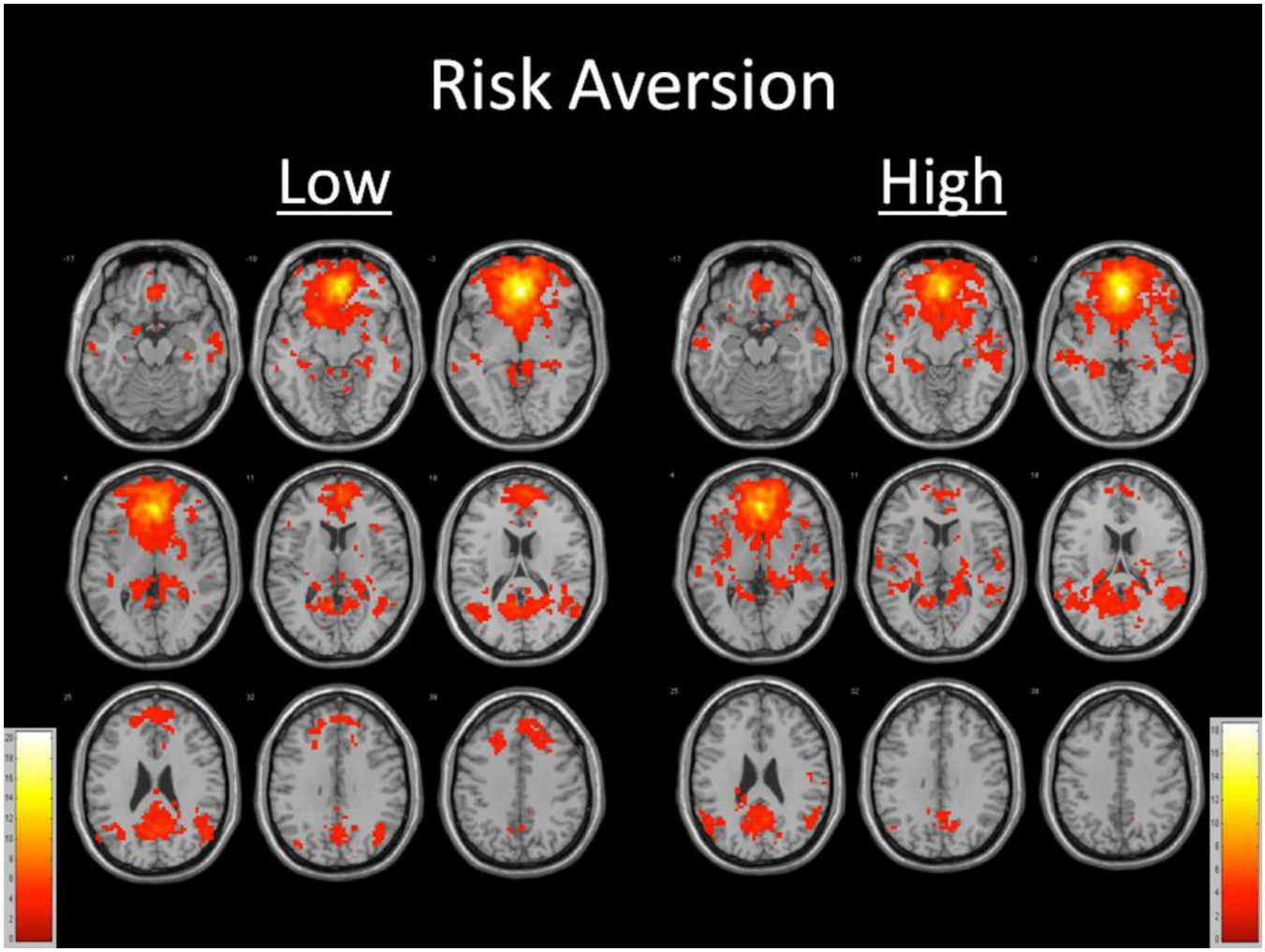

Figure 1.
Functionally connected clusters indicated by a seed region of interest (ROI) prescribed in the ventral anterior cingulate cortex for participants (a) low in gamma (N=27) and participants (b) high in gamma (N=27). Seed ROI MNI coordinates: x=0, y=39, z=−4; radius= 8mm. Adjusted for age and total gray matter volume. False Discovery Rate (FDR) controlled, $p<0.05$. Cluster size > 5 voxels. p-value < 0.004.

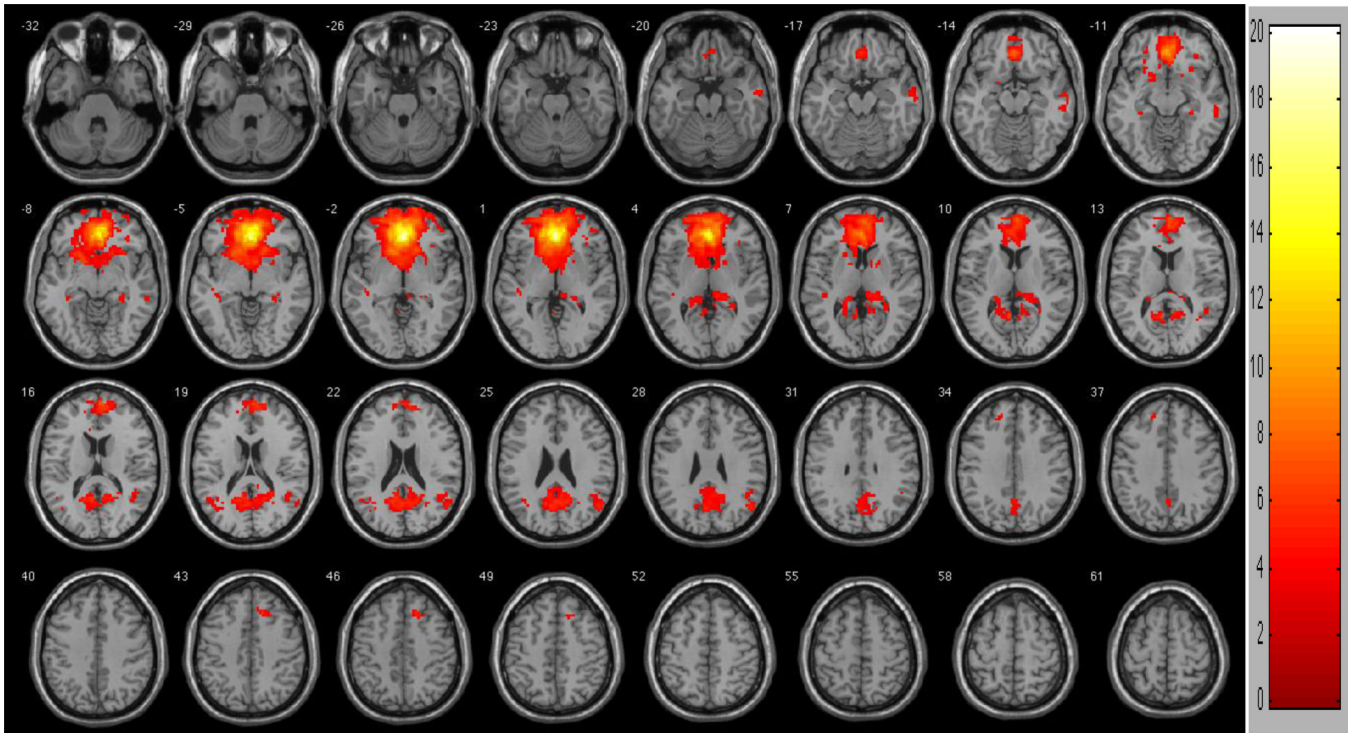

Figure 2.

Regions of similarity between participants low in risk aversion and high in risk aversion. To control for multiple comparisons and spurious findings, we utilized the following congruent with our False Discovery Rate (FDR) controlled within-group analyses: Cluster size > 5 voxels. p-value < 0.004.

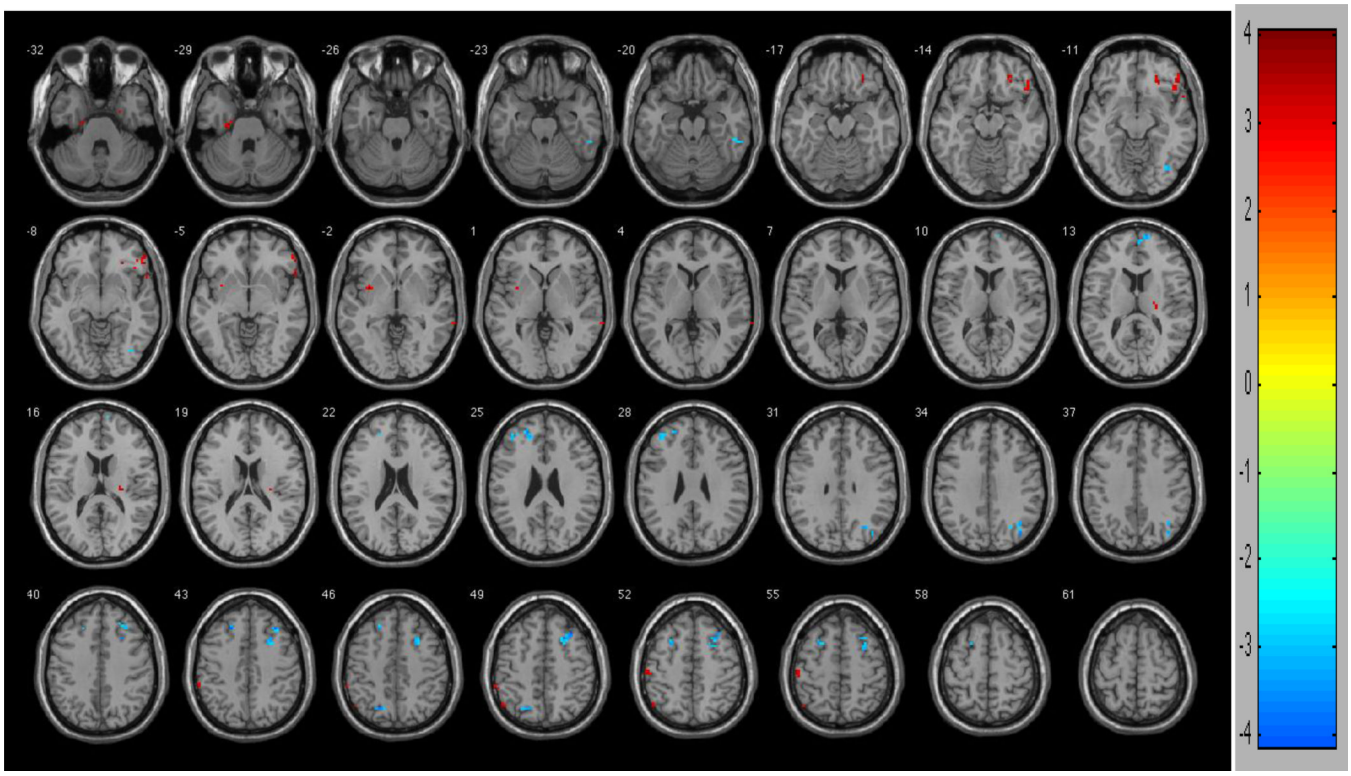

Figure 3.

Regions of contrast between participants low in risk aversion and high in risk aversion. Hot colors (reds) represent regions of difference such that high gamma (high risk aversion) are greater low high gamma (low risk aversion). Cool colors (blues) represent regions of difference such that low gamma (low risk aversion) are greater than high gamma (high risk aversion). To control for multiple comparisons and spurious findings, we utilized the following congruent with our False Discovery Rate (FDR) controlled within-group analyses: Cluster size > 5 voxels. p-value < 0.004.

Table 1

Statistics for demographic, cognitive, gamma (risk aversion), and brain volumetry variables.

	Low Gamma (risk aversion)	High Gamma (risk aversion)	t or X^2	p-value
N	27	27		
Mean Age (SD)	83.98 (6.95)	80.07 (6.56)	2.12	0.03
Education (yrs)	14.85 (2.55)	15.33 (2.81)	−0.65	0.51
Gender (M/F)	20/7	19/8	0.92	0.08
Race (white/other)	27/0	26/1		
MMSE	28.54 (1.17)	28.52 (1.42)	0.56	0.96
Total Gray Matter (mm^3)	282.23 (25.86)	283.42 (25.69)	−0.17	0.87
Estimated Gamma (risk aversion)	0.84(0.07)	3.39 (0.41)	32.16	<0.001

Data are summarized as Mean (Standard deviation=SD) or as number (%). Age and education are presented in years; MMSE is total score; and total gray matter volume is presented as mm^3.

Table 2

Functionally connected clusters as indicated by a seed region of interest (ROI) prescribed in the ventral anterior cingulate cortex and adjusting for the effects of age and total gray matter volume, and results of voxel-wise within-group analyses of z-transformed functional connectivity values while accounting for the effects of age and total gray matter volume.

Gamma	Region	Cluster Size (# voxels)	Maximum Intensity Voxel coordinates			t-value
Low						
	Widespread bilateral frontal, anterior cingulate, basal ganglia, insula, medial temporal, thalamus	3968	0	36	−3	20.1137
	Widespread bilateral temporal, parietal, posterior cingulate, thalamus	1523	−6	−54	9	6.7369
	R middle and superior temporal	295	51	−63	24	5.3182
	R middle temporal	122	60	−9	−18	4.5114
	L medial and superior temporal	80	−45	−27	0	4.4459
	L middle temporal	20	−60	−24	−15	4.0790
	R transverse temporal	5	30	−30	12	3.7896
	L insula	5	−33	−42	18	3.5210
	L middle temporal	8	−54	−9	−9	3.4030
	R cerebellum	5	9	−57	−9	3.4028
	L middle and superior temporal	7	−57	−69	24	3.2940
	R posterior cingulate	8	18	−36	21	3.2873
	R posterior cingulate	8	3	−24	27	3.2484
	R superior temporal	5	42	21	−24	3.2454
	L parahippocampal	5	−24	−45	−12	3.2340
	R superior temporal	5	54	−27	0	3.1343
	L middle temporal	12	−63	−36	−3	3.1224
High						
	Widespread bilateral frontal, temporal, parietal, basal ganglia, insula, anterior and posterior cingulate	5679	0	39	−3	18.8969
	L superior, middle, and inferior temporal	76	−63	−9	−15	4.5704
	R putamen	7	33	−12	6	4.1986
	R parietal	10	48	−9	21	3.8723
	R inferior frontal	11	54	36	−3	3.6893
	R cuneus	13	15	−81	27	3.5766

Gamma	Region	Cluster Size (# voxels)	Maximum Intensity Voxel coordinates			t-value
	L superior temporal	9	−48	−21	12	3.5061
	L thalamus	7	−3	−24	15	3.3787
	R cuneus	11	21	−75	21	3.3529
	R thalamus	5	15	−18	18	2.9456

Seed ROI MNI coordinates: x=0, y=39, z=−4; radius= 8mm. Adjusted for age and total gray matter volume. False Discovery Rate (FDR) controlled, p<0.05. Cluster size > 5 voxels. p-value < 0.004.

Table 3

Functionally connected clusters as indicated by a seed region of interest (ROI) prescribed in the ventral anterior cingulate cortex and adjusting for the effects of age and total gray matter volume, and results of voxel-wise between-group analyses of shared clusters while accounting for the effects of age and total gray matter volume.

Gamma	Region	Cluster Size (# voxels)	Maximum Intensity Voxel coordinates			t-value
Low & High						
	Widespread bilateral frontal, anterior cingulate, basal ganglia, insula, medial temporal, thalamus	3968	0	36	−3	20.1137
	Widespread bilateral temporal, parietal, posterior cingulate, thalamus	1523	−6	−54	9	6.7369
	R middle and superior temporal	295	51	−63	24	5.3182
	R middle temporal	122	60	−9	−18	4.5114
	L medial and superior temporal	80	−45	−27	0	4.4459
	L middle temporal	20	−60	−24	−15	4.0790
	R transverse temporal	5	30	−30	12	3.7896
	L insula	5	−33	−42	18	3.5210
	L middle temporal	8	−54	−9	−9	3.4030
	R cerebellum	5	9	−57	−9	3.4028
	L middle and superior temporal	7	−57	−69	24	3.2940
	R posterior cingulate	8	18	−36	21	3.2873
	R posterior cingulate	8	3	−24	27	3.2484
	R superior temporal	5	42	21	−24	3.2454
	L parahippocampal	5	−24	−45	−12	3.2340
	R superior temporal	5	54	−27	0	3.1343
	L middle temporal	12	−63	−36	−3	3.1224

Seed ROI MNI coordinates: x=0, y=39, z=−4; radius= 8mm. Adjusted for age and total gray matter volume. False Discovery Rate (FDR) controlled, $p<0.05$. Cluster size > 5 voxels. p-value < 0.004.

Table 4

Functionally connected clusters as indicated by a seed region of interest (ROI) prescribed in the ventral anterior cingulate cortex and adjusting for the effects of age and total gray matter volume, and results of voxel-wise between-group analyses for differences in z-transformed functional connectivity values while accounting for the effects of age and total gray matter volume.

Gamma	Region	Cluster Size (# voxels)	Maximum Intensity Voxel coordinates			t-value
Low > High						
	L middle frontal (dorsolateral)	6	−21	30	42	4.0531
	R middle frontal (dorsolateral)	44	33	24	48	4.0050
	R middle frontal (dorsolateral)	10	33	30	42	3.9568
	L superior frontal	12	−21	48	24	3.8265
	R cerebellum	6	39	−60	−39	3.7805
	L superior parietal	8	−21	−66	45	3.7618
	R middle occipital	17	39	−75	33	3.6168
	L superior frontal	8	−27	12	54	3.6092
	R superior medial frontal	11	12	66	12	3.5877
	L middle frontal (dorsolateral)	11	−39	42	27	3.1752
	R inferior occipital	6	39	−69	−12	3.1640
	R inferior temporal	7	54	−39	−21	3.1034
High > Low						
	R parahippocampal	8	24	−3	−36	4.0246
	R inferior frontal	6	57	21	−6	3.5972
	L postcentral	10	−54	−21	54	3.5954
	L parahippocampal	7	−24	−18	−30	3.5574
	L inferior parietal	7	−51	−63	48	3.3627
	R orbital frontal	26	54	33	−9	3.3559
	R middle frontal	13	24	39	−15	3.3498
	L insula	6	−33	3	−3	3.3409
	L precentral	5	−39	−18	66	3.3084
	R thalamus	7	24	−21	15	3.2627
	R middle temporal	5	72	−39	0	3.0381

Gamma	Region	Cluster Size (# voxels)	Maximum Intensity Voxel coordinates			t-value
	L inferior parietal	5	−57	−42	48	2.8866

Seed ROI MNI coordinates: x=0, y=39, z=−4; radius= 8mm. Adjusted for age and total gray matter volume. False Discovery Rate (FDR) controlled, $p<0.05$. Cluster size > 5 voxels. p-value < 0.004.